

Point-DAE: Denoising Autoencoders for Self-supervised Point Cloud Learning

Yabin Zhang¹, Jiehong Lin², Ruihuang Li¹, Kui Jia², Lei Zhang¹

¹Hong Kong Polytechnic University ²South China University of Technology

csybzhang@comp.polyu.edu.hk

Abstract

Masked autoencoder has demonstrated its effectiveness in self-supervised point cloud learning. Considering that masking is a kind of corruption, in this work we explore a more general denoising autoencoder for point cloud learning (Point-DAE) by investigating more types of corruptions beyond masking. Specifically, we degrade the point cloud with certain corruptions as input, and learn an encoder-decoder model to reconstruct the original point cloud from its corrupted version. Three corruption families (i.e., density/masking, noise, and affine transformation) and a total of fourteen corruption types are investigated. Interestingly, the affine transformation-based Point-DAE generally outperforms others (e.g., the popular masking corruptions), suggesting a promising direction for self-supervised point cloud learning. More importantly, we find a statistically significant linear relationship between task relatedness and model performance on downstream tasks. This finding partly demystifies the advantage of affine transformation-based Point-DAE, given that such Point-DAE variants are closely related to the downstream classification task. Additionally, we reveal that most Point-DAE variants unintentionally benefit from the manually-annotated canonical poses in the pre-training dataset. To tackle such an issue, we promote a new dataset setting by estimating object poses automatically. The codes will be available at <https://github.com/YBZh/Point-DAE>.

1. Introduction

Learning effective feature representations from unlabeled data has been attracting growing attention since manual label annotation is labor-intensive and expensive, especially for 3D point cloud data. To this end, self-supervised learning (SSL) techniques have been proposed to generate supervision signals from unlabeled data themselves via carefully designed pretext tasks, such as jigsaw puzzles [22, 30], instance contrastive discrimination [4, 14, 29], and masked autoencoder (MAE)¹ [13, 23, 46]. Among those pre-

text tasks, the effectiveness of MAE has been validated in many applications [13, 23, 35], including point cloud understanding [23, 38, 46]. From the input point clouds masked at a high ratio, an encoder-decoder model is trained to reconstruct the complete point clouds [23, 38, 46]. The pre-trained encoder is then applied to various downstream tasks, while the decoder is typically discarded. Different masking strategies, backbones, and reconstruction targets have been investigated under the MAE framework [19, 23, 38, 49, 50].

Though MAE and its variants have achieved great successes, paying attention only to the masking strategy may limit the capacity of such a generation-based SSL framework. Considering that masking is a kind of corruption, we propose to explore a more general denoising autoencoder [37] for point cloud learning, namely Point-DAE, by investigating more types of corruptions beyond masking. Specifically, we first degrade the point cloud input with certain corruptions, and then learn an encoder-decoder model to reconstruct the uncorrupted input from its corrupted counterpart. We investigate three corruption families, including density/masking, noise, and affine transformation, and hence a total of 14 corruption types, as visualized in Fig. 1. In other words, we study 14 pretext tasks since each corruption instantiates a unique task.

By analyzing these pretext tasks, we find that the affine transformation-based Point-DAE generally outperforms others, such as those based on the popular masking strategies [23, 38], on downstream tasks (please refer to Tab. 1 for details). This finding suggests a promising direction for self-supervised point cloud learning. Taking it a step further, we attribute the advantage of affine transformation-based Point-DAE to its close relatedness to the downstream classification task. More specifically, we measure the task relatedness via the cross-task and within-dataset model transfer performance by following [47]. Such task relatedness defined within the pre-training dataset can statistically predict the SSL performance on downstream tasks, as illustrated in Fig. 2. Compared to other Point-DAE variants, the affine transformation-based Point-DAE presents closer relatedness to the classification task, resulting in better performance on downstream classification

¹We denote by MAE the general autoencoder with masked inputs of different modalities, not only masked 2D images [13].

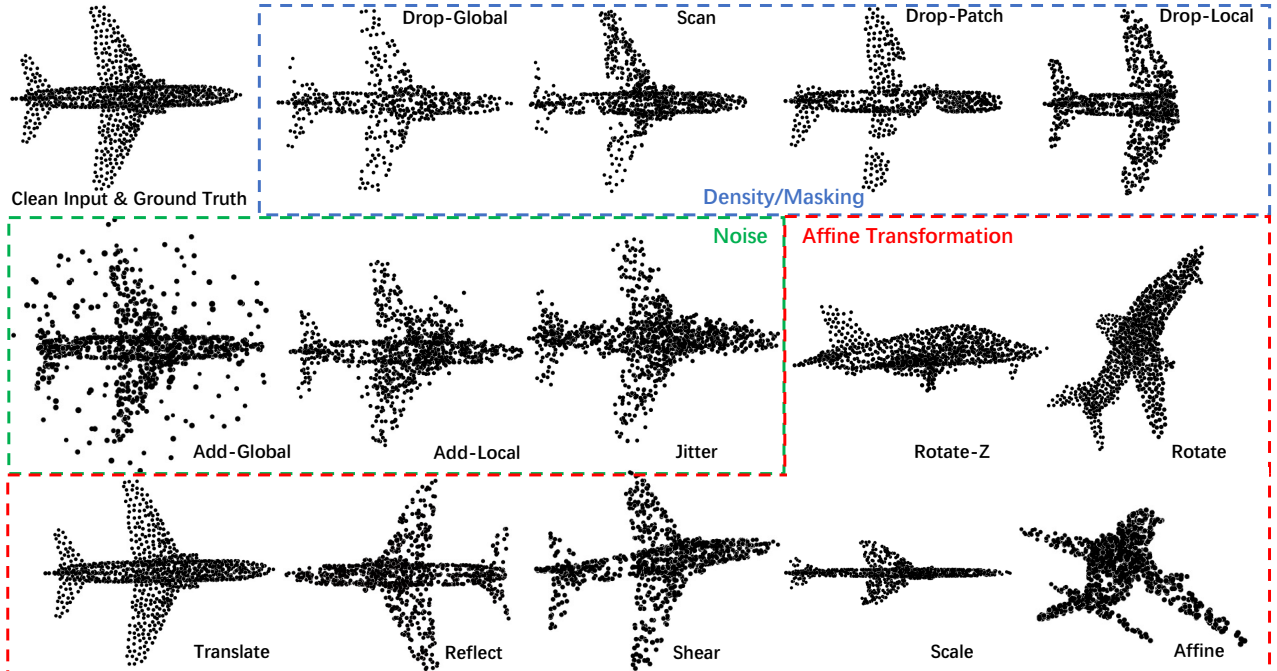


Figure 1. Illustration of the 14 corruptions studied in this work, which can be classified into three corruption families, *i.e.*, density/masking, noise, and affine transformation. Please refer to the **supplementary material** for more detailed implementation of these corruptions.

tasks. Furthermore, by taking advantage of both affine transformation and local masking corruptions, we can empower Point-DAE with higher relatedness to classification and improve the downstream classification performance.

Lastly, we reveal that most Point-DAE variants unintentionally benefit from the manually-annotated canonical poses in the pre-training datasets. More specifically, samples of the same category are manually assigned with a category-canonical pose in existing pre-training datasets [3, 40]. Though the category label is not explicitly utilized, such manually aligned category-canonical poses implicitly carry the manual category annotation. Most Point-DAE variants more or less benefit from such manual poses unintentionally (please refer to Fig. 6 for more details). To eliminate such manual annotations from the self-supervised pre-training, we promote a new dataset setting by automatically estimating object poses with singular value decomposition (SVD) [52]. Without the effect of manual poses, the new dataset setting could more faithfully evaluate and guide the self-supervised point cloud learning methods.

2. Related Work

Self-supervised point cloud learning. SSL aims to learn effective feature representations from unlabeled data with supervision signals generated from the data themselves [4, 14]. Many SSL methods (*e.g.*, contrastive learning [27, 29], reconstruction [23, 38, 43, 46], and so on [1, 24, 30]) have been proposed for the point cloud learning tasks, while

the MAE framework has been attracting growing attention due to its simplicity and effectiveness [23, 38]. In this paper, we explore a more general Point-DAE framework beyond MAE. Actually, similar ideas have been considered in previous studies. For example, in the 2D image domain, the denoising autoencoder (DAE) [37] has been proposed to reconstruct a clean image from its “corrupted” version; however, only the masking corruption is validated. Recently, Tian *et al.* [34] investigated the DAE framework in the 2D image domain with six corruptions including masking. In their study, masking is found to be the most effective corruption and combining masking with other corruptions leads to marginal improvement. In the 3D point cloud domain, corruptions beyond masking have also been attracting increasing attention. For instance, corruptions of downsampling [48], part disorganization [5], and contour perturbation [42] have been individually investigated.

In this work, we systematically investigate Point-DAE with a variety of corruption types. Two interesting findings are made in our studies. Firstly, the affine transformation-based Point-DAE generally outperforms its counterparts with other corruptions in point cloud learning. Secondly and more importantly, a statistically significant linear relationship exists between task relatedness and SSL performance on downstream tasks, partly demystifying the advantage of affine transformation-based Point-DAE.

Sample corruptions. Sample corruptions have been widely investigated in different research areas. Data aug-

mentation via sample corruptions has demonstrated its effectiveness in settings of both independent and identical distribution [6, 7] and our-of-distribution (OOD) [16]. The dataset for testing OOD generalization performance is typically generated by applying corruptions to clean samples [15, 28]. Sample corruptions also play important roles in semi-supervised learning [32] and contrastive learning [4]. In low-level vision tasks (e.g., image super-resolution [8] and point cloud upsampling [45]), training pairs are typically constructed by applying corruptions to high-quality samples. However, the objective in low-level vision tasks is mainly to reconstruct high-quality samples, while the main objective of SSL is to learn effective feature representations without manual annotations.

Task relatedness. Task relatedness is one of the key problems in multi-task learning [51]. By learning related and cooperative tasks together, we can share useful knowledge across tasks, improve the performance of all tasks, and achieve the desired performance with fewer training samples [47, 51]. We investigate the task relatedness between pretext tasks and the downstream target task by instantiating Point-DAE with various corruptions as different pretext tasks. In multi-task learning, the multiple tasks are typically defined on the same dataset, while datasets used for the pretext and downstream tasks in SSL are typically different. Interestingly, as shown in Fig. 2, the task relatedness within the pre-training dataset can statistically predict the SSL performance on downstream tasks, providing a useful signal for the pretext task selection.

3. Point-DAE and Task Relatedness

3.1. Point-DAE with Different Corruptions

Given a point cloud dataset X with unlabeled samples, we explore the following Point-DAE framework:

$$\min_{E, D} \mathbb{E}_{\mathbf{x} \in X} \mathcal{L}(D(E(C(\mathbf{x}))), \mathbf{x}), \quad (1)$$

where \mathbf{x} is a sample in X . C indicates the applied corruption (e.g., masking and random noise). E and D represent the encoder and decoder models, respectively. \mathcal{L} is the loss function measuring the reconstruction quality, which is set as the popular Chamfer Distance [11] in this work. We investigate the Point-DAE with different encoder architectures, such as multilayer perceptron (MLP) [25, 26] and graph neural network [39], and instantiate the decoder with the effective FoldingNet [43].

The corruption C is our focus in this work, given that each type of corruption instantiates a unique pretext task. Inspired by the practice of [28, 33], we systemically investigate three corruption families (i.e., density/masking, noise, and affine transformation) and a total of 14 corruption types. Generally speaking, we randomly change the point density either uniformly or nonuniformly to implement the

density/masking corruptions, and add random noises to the point cloud either locally or globally to implement the noise corruptions. The affine transformation corruptions are implemented by multiplying the augmented input with a random affine transformation matrix as follows:

$$\begin{bmatrix} x' \\ y' \\ z' \\ 1 \end{bmatrix} = \begin{bmatrix} a_{11} & a_{12} & a_{13} & a_{14} \\ a_{21} & a_{22} & a_{23} & a_{24} \\ a_{31} & a_{32} & a_{33} & a_{34} \\ 0 & 0 & 0 & 1 \end{bmatrix} \begin{bmatrix} x \\ y \\ z \\ 1 \end{bmatrix}, \quad (2)$$

where $[x, y, z]$ and $[x', y', z']$ are the input and transformed points, respectively. The affine transformation matrix is defined by the 12 parameters, i.e., a_{ij} .

The representative corruptions are visualized in Fig. 1. One can see that we implement four corruptions for density/masking family, three corruptions for noise family, and seven corruptions for affine transformation family, resulting in 14 types of corruptions in total.

3.2. Task Relatedness Measurement

Without loss of generality, we adopt the point cloud classification as the target downstream task and analyze its relatedness with the 14 pretext tasks induced by the 14 types of corruptions. Following [47], we first conduct task-specific modeling by training each pretext task in a fully supervised manner with self-supervised pre-training (the details of pre-training can be found in Sec. 4.1). For each pretext task c , Zamir *et al.* [47] defined its task relatedness to the downstream task t as:

$$\hat{A}_{c \rightarrow t} := \min_R \mathbb{E}_{\mathbf{x} \in X} \mathcal{L}_t(R(E_c(\mathbf{x})), f_t(\mathbf{x})), \quad (3)$$

where E_c is the pre-trained encoder on task c with Eq. (1), and R , f_t , and \mathcal{L}_t are a small readout function, the labeling function, and the loss function for task t , respectively. $\hat{A}_{c \rightarrow t}$ measures whether the feature representation $E_c(\mathbf{x})$ learned with task c is sufficient for solving task t , which is a practical metric for task relatedness. For classification task t , we construct R with one fully connected (FC) layer, adopt f_t as the category labeling function, and instantiate \mathcal{L}_t with the popular cross-entropy loss.

In practice, there exists certain inconsistency between the loss value and classification accuracy. Considering that we attach more importance to the accuracy than loss value in the performance evaluation, we slightly modify the task relatedness defined in Eq. (3) by replacing the loss value with the accuracy measurement:

$$A_{c \rightarrow t} := \mathbb{E}_{\mathbf{x} \in X} \mathcal{I}(R_c(E_c(\mathbf{x})), f_t(\mathbf{x})), \quad (4)$$

where R_c is the readout function learned with Eq. (3), and $\mathcal{I}(R_c(E_c(\mathbf{x})), f_t(\mathbf{x}))$ measures whether the model prediction $\mathcal{I}(R_c(E_c(\mathbf{x})))$ agrees with the labeling function $f_t(\mathbf{x})$. The accuracy-based task relatedness performs better under

the accuracy-dominated evaluation context. More details can be found in the **supplementary material**.

One may consider that the task relatedness defined in Eq. (4) is similar to the linear classification fine-tuning protocol detailed in Sec. 4.3. We clarify that there are two major differences. Firstly, task relatedness measurement and pretext task learning are conducted on the same dataset, while the datasets for downstream tasks are usually different from that used in pre-training. Secondly, only a small number of samples are utilized for training R , since whether the transferable knowledge is easily accessible is vital for the task relatedness measurement [47].

4. Experiments

We conduct extensive experiments to investigate the performance of different variants of Point-DAE, which are corresponding to different types of corruptions, on the classification task of point cloud learning.

4.1. Self-supervised Pre-training

Following [23, 46], we conduct self-supervised point cloud learning on the ShapeNet dataset [3], which contains about 51K samples shared by 55 categories. We adopt the popular PointNet [25], PointNet++ [26], and DGCNN [39] as the encoder, and instantiate the FoldingNet [43] as the decoder following the practice of [38]. We adopt a light-weighted PointNet architecture by removing the transformation modules since the transformation modules (*i.e.*, T-Net) in PointNet are incompatible with the affine transformation corruption (refer to Sec. 4.4 for more details). Besides the Point-DAE variants induced by the 14 analyzed corruptions, we introduce the vanilla autoencoder (*i.e.*, Point-DAE with ‘No-Corruption’ input) as the baseline, and explore the Point-DAE variants with combined corruptions. To compare Point-DAE with supervised pre-training, we introduce the ‘Supervised’ setting by learning the encoder with manual category labels.

We adopt the AdamW optimizer [21] and use the cosine learning rate schedule [20]. The total training epochs, initial learning rate, and number of points are respectively set as 300, 0.001, and 1024 unless otherwise specified. We adopt the same experimental setting across different backbones and Point-DAE variants to ensure a fair comparison.

4.2. Task Relatedness vs. SSL Performance

Given the pre-trained models, we first investigate the relationship between SSL performance and task relatedness, which is defined between the pretext and downstream tasks in Eq. (4). We adopt the Pearson correlation coefficient (*i.e.*, $r \in (-1, 1)$) to measure the linear relationship and utilize the p -value (*i.e.*, $p \in (0, 1)$) to measure the statistical significance for the Pearson correlation [2, 10]. Generally,

	Corruptions	PointNet	PointNet++	DGCNN
	▼ No-Corruption	75.7±0.9	76.2±0.9	77.1±0.3
Density	♣ Drop-Global	74.4±0.2	77.3±0.5	76.4±0.2
	♣ Scan	77.0±0.1	78.1±1.2	78.9±0.3
	♣ Drop-Patch	72.7±0.4	80.6±1.1	77.4±1.0
	♣ Drop-Local	73.6±0.4	78.5±0.7	80.8±0.8
Noise	◆ Add-Global	73.6±0.3	77.5±0.6	77.3±0.9
	◆ Add-Local	74.9±0.7	76.5±0.5	77.2±0.3
	◆ Jitter	76.0±0.8	76.1±0.3	78.0±1.4
Affine Trans.	♠ Shear	75.6±0.1	77.7±0.1	79.4±0.6
	♠ Rotate-Z	73.9±0.4	77.9±0.3	79.2±0.9
	♠ Translate	75.1±0.4	78.6±0.1	81.2±0.7
	♠ Scale	77.2±0.9	79.9±0.5	80.4±0.5
	♠ Reflect	78.3±0.7	81.8±0.3	82.8±0.3
	♠ Rotate	76.2±0.1	80.6±0.8	82.8±0.5
	♠ Affine	77.4±0.7	84.9±1.0	84.4±0.3
Comb.	Affine			
	★ + Drop-Patch	74.8±0.1	86.0±0.6	84.8±0.1
	★ + Drop-Local	75.6±0.5	87.0±0.7	85.5±0.7
	■ Supervised	78.3±0.2	87.0±0.1	86.8±0.2

Table 1. Results of different variants of Point-DAE on the ScanObjectNN dataset with the ObjBG setting. The linear classification protocol is used.

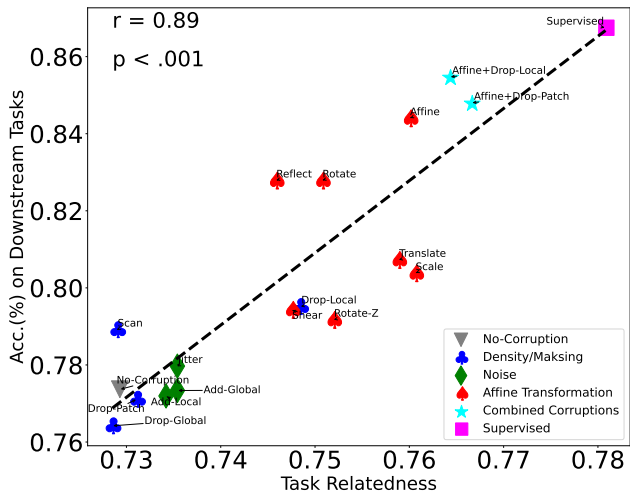


Figure 2. Illustration of the statistically significant linear relationship (*i.e.*, $r = 0.89$ and $p < .001$) between the task relatedness and classification accuracy on downstream tasks. We adopt the DGCNN model as the encoder and report results on the ObjBG setting of ScanObjectNN dataset under the linear classification protocol. Please zoom in for the exact name of each point.

$|r| > 0.5$ indicates a strong relationship and $p < 0.05$ describes the statistical significance. The results of Point-DAE variants are shown in Tab. 1 and their relationships to task relatedness are visualized in Fig. 2. Results and visualizations with more backbones and downstream tasks can be found in the **supplementary material**. From these studies, we can have the following two interesting findings.

First, there exists a statistically significant linear rela-

relationship between task relatedness and SSL performance (*e.g.*, $p < .001$). Specifically, the Point-DAE variants with closer task relatedness to classification could achieve better downstream classification performance with a higher probability. Second, compared with other corruptions, affine transformation-based Point-DAE typically holds closer task relatedness to point cloud classification, leading to higher accuracy on downstream classification tasks.

Besides the above general findings, we observe that the task relatedness also depends on model architectures. For instance, the popular local point masking strategy (*e.g.*, Drop-Patch or Drop-Local) leads to different results with different model architectures. For PointNet++ and DGCNN, which are designed with local perception modules, randomly masking local part of the input introduces explicit regularization, benefiting the extraction and aggregation of local features. Therefore, their task relatedness to classification can be enhanced with corruptions of local point masking. On the contrary, masking local points brings a significant negative impact on PointNet, where the global information is overly weighted than local knowledge. Similarly, empowering Affine corruption with local point masking generally leads to better results for PointNet++ and DGCNN backbones, whereas this generally results in degenerated performance for PointNet, as shown in Tab. 1. In the following experiments, we adopt Affine+Drop-Local as the default corruption for PointNet++ and DGCNN, while Affine is adopted for PointNet. Such settings generally work well but not necessarily achieve the best results under the Point-DAE framework.

4.3. Fine-tuning on Downstream Tasks

We adopt the following two protocols to validate the pre-trained encoder on downstream tasks:

- Transferring features protocol, where we fine-tune both the pre-trained encoder and the randomly initialized classification head on downstream tasks.
- Linear classification protocol, where we freeze the pre-trained encoder and learn a linear support vector machine (SVM) classifier on the extracted features.

In the following studies, results of competitors are either copied from the original papers or quoted from [1, 38]. Besides vanilla Point-DAE (*i.e.*, Point-DAE (Ours)), we also report the results on an SVD-Pose pre-training dataset (*i.e.*, Point-DAE (SVD-Pose)), which is detailed in Sec. 5.

Object classification on real-world dataset. There is a high demand for transferring the pre-trained models to real-world point cloud tasks, since the point cloud sample collection and annotation is time-consuming and expensive. Therefore, we first validate our method on the real-world ScanObjectNN dataset [36]. Following [1, 38], we adopt the OBJ-BG setting, which includes about 2.8K samples shared by 15 categories. As illustrated in Tab. 2, our Point-DAE

Methods	#Points	PointNet	DGCNN
Linear Classification Protocol			
Jigsaw [30]	–	55.2	59.5
OcCo [38]	1K	69.5	78.3
CrossPoint [1]	1K	75.6	81.7
Point-DAE (Ours)	1K	78.1±0.3	87.9±0.2
Point-DAE (SVD-Pose)	1K	77.8±0.1	82.4±0.9
Transferring Features Protocol			
From Scratch	1K	73.3	82.4
Jigsaw [30]	1K	76.5±0.4	82.7±0.8
OcCo [38]	1K	80.0±0.2	83.9±0.4
Point-DAE (Ours)	1K	80.2±0.2	92.1±0.2
Point-DAE (SVD-Pose)	1K	80.2±0.2	89.9±0.3

Table 2. Classification results on the ScanObjectNN dataset.

Methods	#Points	PointNet	DGCNN
Linear Classification Protocol			
Self-Contrast [9]	1K	–	89.6
OcCo [38]	1K	88.7	89.2
Jigsaw [30]	–	87.3	90.6
Poursaeed <i>et al.</i> [24]	1K	88.6	90.8
STRL [17]	2K	88.3	90.9
CrossPoint [1]	1K	89.1	91.2
Point-DAE (Ours)	1K	89.3±0.1	91.9±0.2
Point-DAE (SVD-Pose)	1K	89.0±0.1	90.7±0.1
Transferring Features Protocol			
From Scartch	1K	89.2±0.1	92.5±0.4
Jigsaw [30]	1K	89.6±0.1	92.3±0.3
OcCo [38]	1K	90.1±0.1	93.0±0.2
STRL [17]	–	–	93.1
Point-DAE (Ours)	1K	90.6±0.1	93.3±0.1
Point-DAE (SVD-Pose)	1K	90.6±0.1	93.0±0.1

Table 3. Classification results on ModelNet40 dataset.

significantly outperforms its competitors with popular backbones of PointNet and DGCNN under the two fine-tuning protocols. Notably, Point-DAE achieves 87.9% with the DGCNN backbone, outperforming the CrossPoint by 6.2% under the linear classification protocol.

Object classification on synthetic dataset. We then validate Point-DAE on the synthetic dataset of ModelNet40 [40], which includes 12,311 clean samples shared by 40 categories. The standard split of training and test data is adopted. As shown in Tab. 3, Point-DAE outperforms all competitors with PointNet and DGCNN backbones. Compared to the results on the challenging real-world dataset in Tab. 2, the improvement of our method is smaller on the synthetic ModelNet40 dataset, mainly because clean sample recognition is much easier.

Few-shot classification. We evaluate Point-DAE with few-shot classification on datasets of ModelNet-40 and ScanObjectNN. The ‘ n -way, m -shot’ setting is adopted, where n is the number of randomly selected categories and

	5-way		10-way	
	10-shot	20-shot	10-shot	20-shot
PointNet: Transferring Features Protocol				
From Scratch [25]	52.0±3.8	57.8±4.9	46.6±4.3	35.2±4.8
Jigsaw [30]	66.5±2.5	69.2±2.4	56.9±2.5	66.5±1.4
cTree [31]	63.2±3.4	68.9±3.0	49.2±1.9	50.1±1.6
OcCo [38]	89.7±1.9	92.4±1.6	83.9±1.8	89.7±1.5
CrossPoint [1]	90.9±4.8	93.5±4.4	84.6±4.7	90.2±2.2
Point-DAE (Ours)	93.0±3.7	94.9±3.3	86.7±5.8	92.1±4.6
Point-DAE (SVD-Pose)	92.1±4.6	94.9±3.6	86.3±4.9	91.3±4.4
DGCNN: Transferring Features Protocol				
From Scratch [39]	31.6±2.8	40.8±4.6	19.9±2.1	16.9±1.5
Jigsaw [30]	34.3±1.3	42.2±3.5	26.0±2.4	29.9±2.6
cTree [31]	60.0±2.8	65.7±2.6	48.5±1.8	53.0±1.3
OcCo [38]	90.6±2.8	92.5±1.9	82.9±1.3	86.5±2.2
CrossPoint [1]	92.5±3.0	94.9±2.1	83.6±5.3	87.9±4.2
Point-DAE (Ours)	96.7±2.5	97.7±1.6	93.0±4.8	95.6±2.6
Point-DAE (SVD-Pose)	95.3±2.9	97.5±1.8	91.7±3.9	94.8±3.2
(a) ModeNet40				
	5-way		10-way	
	10-shot	20-shot	10-shot	20-shot
PointNet: Transferring Features Protocol				
From Scratch [25]	57.6±2.5	61.4±2.4	41.3±1.3	43.8±1.9
Jigsaw [30]	58.6±1.9	67.6±2.1	53.6±1.7	48.1±1.9
cTree [31]	59.6±2.3	61.4±1.4	53.0±1.9	50.9±2.1
OcCo [38]	70.4±3.3	72.2±3.0	54.8±1.3	61.8±1.2
CrossPoint [1]	68.2±1.8	73.3±2.9	58.7±1.8	64.6±1.2
Point-DAE (Ours)	71.3±6.9	74.5±5.7	59.6±3.7	66.2±4.5
Point-DAE (SVD-Pose)	69.6±3.1	73.2±2.8	58.4±1.7	65.0±2.1
DGCNN: Transferring Features Protocol				
From Scratch [39]	62.0±5.6	67.8±5.1	37.8±4.3	41.8±2.4
Jigsaw [30]	65.2±3.8	72.2±2.7	45.6±3.1	48.2±2.8
cTree [31]	68.4±3.4	71.6±2.9	42.4±2.7	43.0±3.0
OcCo [38]	72.4±1.4	77.2±1.4	57.0±1.3	61.6±1.2
CrossPoint [1]	74.8±1.5	79.0±1.2	62.9±1.7	73.9±2.2
Point-DAE (Ours)	84.5±4.5	88.2±5.3	76.4±1.9	81.6±2.4
Point-DAE (SVD-Pose)	77.9±7.3	81.7±7.3	66.4±3.0	75.6±2.4
(b) ScanObjectNN				

Table 4. Few-shot classification results with 1K input points.

m is the number of training samples in each category. For each class, 20 additional samples are selected as test data. Results of each setting are reported with 10 random experiments. As illustrated in Tab. 4, Point-DAE significantly outperforms the competitors with PointNet and DGCNN backbones. Such advantages justify that knowledge can be more easily transferred with our Point-DAE.

Part segmentation. The ShapeNetPart dataset [44], which is composed of 16 classes and 16,881 samples, is adopted in this experiment. We follow [38] to construct the segmentation decoder. As presented in Tab. 5, Point-DAE outperforms its competitors with PointNet and DGCNN backbones. Though Point-DAE is proposed for downstream classification tasks, it also achieves good performance on

Methods	#Points	PointNet	DGCNN
From Scratch	2K	82.2	85.2
OcCo [38]	2K	83.4	85.0
Jigsaw [30]	–	–	85.1
PointContrast [41]	2K	–	85.3
CrossPoint [1]	2K	–	85.5
Chen <i>et al.</i> [5]	2K	84.1	–
Point-DAE (Ours)	2K	84.7±0.1	85.9±0.1
Point-DAE (SVD-Pose)	2K	84.4±0.1	85.7±0.1

Table 5. Part segmentation results of mean IoU across all object classes on the ShapeNetPart dataset, where the transferring features protocol is adopted.

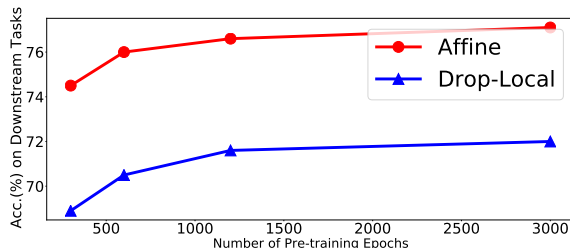


Figure 3. Performance of Point-DAE variants with different number of pre-training epochs. Results are reported on the PB-T50-RS setting of ScanobjectNN dataset with DGCNN backbones.

part segmentation, possibly due to the close task relatedness between classification and part segmentation.

4.4. Discussions

Pre-training epochs. It is noted that existing point cloud learning methods pay less attention to the number of pre-training epochs, and different methods adopt different epochs, impeding the fair comparison among them. As illustrated in Fig. 3, the Affine-based Point-DAE consistently outperforms its counterpart with the Drop-Local corruption under various pre-training epochs, illustrating the advantage of Affine corruption in the Point-DAE framework. Higher accuracy on downstream tasks is typically achieved with a larger number of pre-training epochs. In the paper, we set the number of pre-training epochs as 300 in all experiments except these in Sec. 4.3, where we pre-train the Point-DAE model for 1, 200 epochs.

Transformation module. As shown in Tab. 6, the transformation module (*i.e.*, T-Net) in PointNet [25] is incompatible with the affine transformation corruption. This conflict may come from the intrinsic transformation rectification mechanism in T-Net, which dilutes the influence of affine transformation. We adopt the PointNet w/o T-Net as the default PointNet implementation. Although our adopted PointNet uses fewer parameters, it still significantly outperforms other competitors, as shown in Sec. 4.3.

Reconstruction targets. Given corrupted input, instead of reconstructing its uncorrupted version with Point-DAE, we may reconstruct the corrupted sample itself under the

Methods	#Params	Acc. (%)
PointNet with T-Net	3.5M	73.8
PointNet w/o T-Net (our adopted)	0.8M	77.4

Table 6. Results of our Point-DAE on the ObjBG setting of ScanObjectNN dataset, where the Affine corruption is adopted.

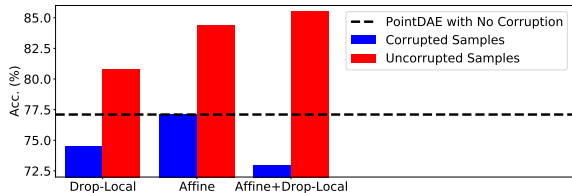


Figure 4. Classification results on the ObjBG setting of ScanObjectNN dataset with different reconstruction targets.

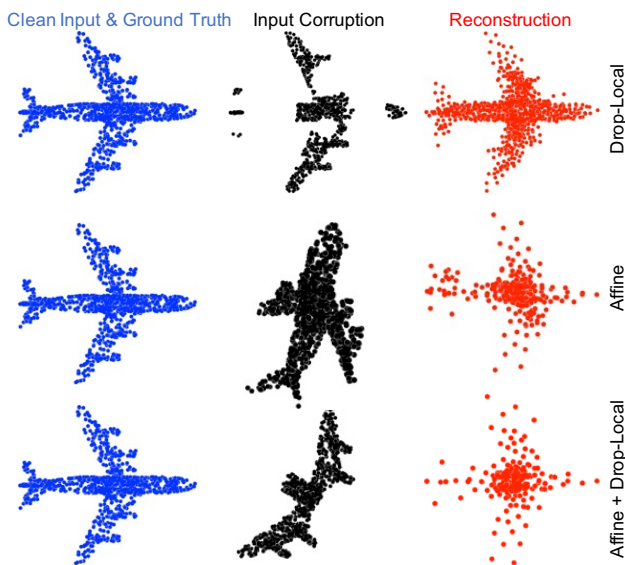


Figure 5. Reconstruction visualization on ShapeNet validation set with three Point-DAE variants. Qualitative visualization and quantitative analyses on reconstruction performance with more Point-DAE variants can be found in the **supplementary material**.

vanilla autoencoder framework. As shown in Fig. 4, reconstructing the uncorrupted samples presents a substantial advantage. This validates that the advantage of Point-DAE originated from the anti-corruption reconstruction, rather than the data diversity augmented by corruptions.

Visualization. As illustrated in Fig. 5, the Affine-related Point-DAE reconstructs the overall shape of point clouds, capturing the category concept. Although the Drop-Local based Point-DAE performs better on the reconstruction performance, the Affine-related Point-DAE achieves clear advantages on downstream tasks as shown in Tab. 1, presenting the divergence between tasks of reconstruction and SSL.

Time complexity. All Point-DAE variants share almost the same training and test complexity, since they are only different in the used corruptions, which could be conducted with the dataloader in a parallel manner.

5. Revisiting the Datasets

While the affine transformation-based Point-DAE shows close task relatedness to classification and significantly outperforms its competitors on downstream classification tasks, we take a further step and find that such advantages partly stem from one limitation of the current point cloud datasets. More precisely, in those popular pre-training datasets such as ShapeNet [3] and ModelNet [40], samples are manually aligned to category-wise canonical poses. In other words, the canonical poses have implicitly carried the manual category annotation, which is unintentionally utilized by the SSL algorithms, including the Point-DAE variants (please refer to Fig. 6 for more illustrations). This does not conform to the practical requirement that we should not manually assign an unlabeled sample with any category-aware canonical pose.

5.1. Dataset without Manual Poses

To overcome the dataset limitation discussed above, one intuitive solution is to assign each point cloud with a random pose, leading to the ‘Random-Pose’ setting. However, pose plays an important role in point cloud understanding [18, 52] and it should not be neglected. To make appropriate use of the information of poses, we propose to automatically estimate the canonical pose for each sample with the singular value decomposition (SVD) strategy [12, 52], resulting in the ‘SVD-Pose’ setting, where poses of samples in the same category are roughly aligned without any manual effort. In contrast, the vanilla dataset with manual poses is termed as ‘Manual-Pose’.

5.2. Point-DAE on Dataset with SVD-Pose

Results with different dataset settings. We illustrate the results of Point-DAE on different dataset settings in Fig. 6. We have the following three findings.

First, it is not a surprise that the models pre-trained on the Manual-Pose setting typically achieve the best results since they benefit from the manually labeled information, which should not be used under the SSL paradigm. The models pre-trained under the SVD-Pose setting generally outperform their counterparts with Random-Pose, demonstrating the effectiveness of automatic pose estimation.

Second, the Point-DAE variants more or less benefit from the aligned poses, including the vanilla autoencoder, the autoencoder with masked input, and other variants. Especially, the Point-DAE with Reflect, Rotate, and Affine corruptions gain more benefits from the aligned poses because these corruptions significantly distort the poses.

Third, though dropping the manual poses degenerates the performance of most Point-DAE variants, the Point-DAE with Affine corruption still outperforms its competitors with other corruptions. In addition, combining Affine

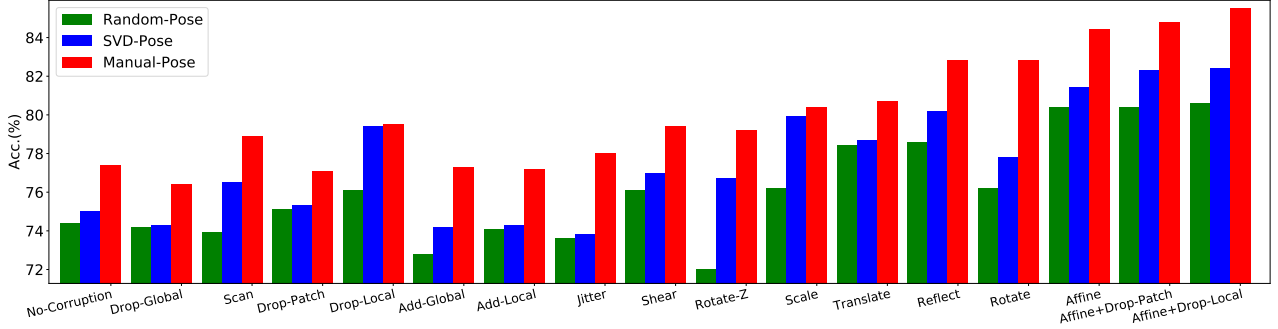


Figure 6. Results of Point-DAE with different pre-training datasets with and without manual poses. Experiments are conducted on the ObjBG setting of ScanObjectNN dataset under the linear classification protocol with the DGCNN backbone. Similar results with more backbones and downstream tasks are provided in the **supplementary material**.

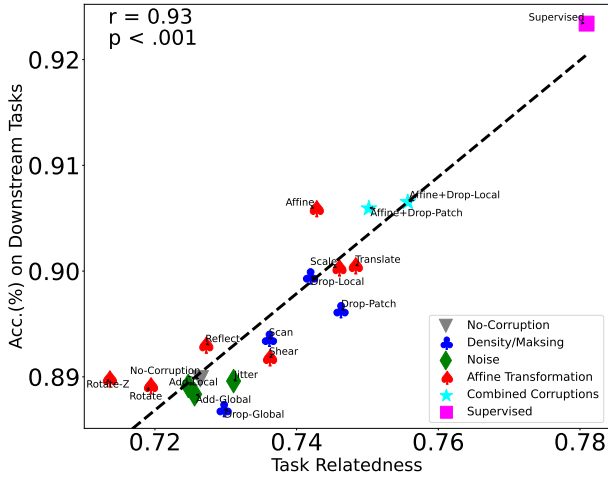


Figure 7. Illustration of the statistically significant linear relationship (*i.e.*, $r = 0.93$ and $p < .001$) between the task relatedness and classification accuracy on downstream tasks, where the pre-training is conducted on the SVD-Pose setting. We adopt the DGCNN model as the encoder and report results on the ModelNet40 dataset under the linear classification protocol. Results with more encoders and downstream tasks are provided in the **supplementary material**.

and local point masking strategies (*i.e.*, Drop-Local and Drop-Patch) further boosts the performance, which is consistent with the observations on the Manual-Pose setting.

We promote the new dataset setting with SVD-Pose for self-supervised point cloud learning, since this setting not only eliminates the manual pose annotation but also preserves the valuable pose information to some extent.

Task relatedness. We revisit the relationship between task relatedness and performance on downstream tasks under the SVD-Pose setting. As illustrated in Fig. 7, similar findings to the Manual-Pose setting in Fig. 2 can be made. That is, the statistically significant linear relationship between the task relatedness and performance on downstream tasks also holds (*i.e.*, $r = 0.93$ and $p < .001$).

Downstream results with pre-training dataset of SVD-Pose.

Given the model pre-trained with the SVD-Pose setting, we revisit the downstream tasks following the same strategy as in Sec. 4.3. Downstream results on the classification of real-world and synthetic samples, few-shot classification, and part segmentation are respectively illustrated in Tab. 2, Tab. 3, Tab. 4, and Tab. 5 with the name of Point-DAE (SVD-Pose). Although the results of Point-DAE (SVD-Pose) are mostly lower than those of Point-DAE (Ours), a significant improvement over the ‘From Scratch’ baseline is achieved with the SVD-Pose setting, validating the effectiveness of self-supervised pre-training. Moreover, our Point-DAE (SVD-Pose) achieves comparable or better performance than the competing non-Point-DAE methods pre-trained with the Manual-Pose setting, justifying the effectiveness of our Point-DAE method.

6. Conclusion

We comprehensively investigated the Point-DAE model with 14 corruption types. Among these corruptions, the affine transformation presented clear advantages over the prevalent masking corruption, at least for downstream point cloud classification tasks. Furthermore, we revealed a statistically significant linear relationship between task relatedness and performance on downstream tasks, which suggests a selection guideline for the pretext task without accessing to data of downstream tasks. We also pointed out that most existing point cloud learning methods may unintentionally benefit from the manually canonical poses in the pre-training dataset. Therefore, we promoted a new dataset setting by estimating object poses automatically. Under this setting, the advantages of our Point-DAE still held. In the future work, we will investigate the Point-DAE models with the transformer backbones [19,23,46], where the corruption is conducted at the local patch level, and include other SSL frameworks (*e.g.*, contrastive learning [27,29]) in the study.

References

- [1] Mohamed Afham, Isuru Dissanayake, Dinithi Dissanayake, Amaya Dharmasiri, Kanchana Thilakarathna, and Ranga Rodrigo. Crosspoint: Self-supervised cross-modal contrastive learning for 3d point cloud understanding. *arXiv preprint arXiv:2203.00680*, 2022. 2, 5, 6
- [2] Sarah Boslaugh. *Statistics in a nutshell: A desktop quick reference*. ” O’Reilly Media, Inc.”, 2012. 4
- [3] Angel X. Chang, Thomas Funkhouser, Leonidas Guibas, Pat Hanrahan, Qixing Huang, Zimo Li, Silvio Savarese, Manolis Savva, Shuran Song, Hao Su, Jianxiong Xiao, Li Yi, and Fisher Yu. ShapeNet: An Information-Rich 3D Model Repository. Technical Report arXiv:1512.03012 [cs.GR], Stanford University — Princeton University — Toyota Technological Institute at Chicago, 2015. 2, 4, 7
- [4] Ting Chen, Simon Kornblith, Mohammad Norouzi, and Geoffrey Hinton. A simple framework for contrastive learning of visual representations. In *International conference on machine learning*, pages 1597–1607. PMLR, 2020. 1, 2, 3
- [5] Ye Chen, Jinxian Liu, Bingbing Ni, Hang Wang, Jiancheng Yang, Ning Liu, Teng Li, and Qi Tian. Shape self-correction for unsupervised point cloud understanding. In *Proceedings of the IEEE/CVF International Conference on Computer Vision*, pages 8382–8391, 2021. 2, 6
- [6] Ekin D Cubuk, Barret Zoph, Dandelion Mane, Vijay Vasudevan, and Quoc V Le. Autoaugment: Learning augmentation strategies from data. In *Proceedings of the IEEE/CVF Conference on Computer Vision and Pattern Recognition*, pages 113–123, 2019. 3
- [7] Ekin D Cubuk, Barret Zoph, Jonathon Shlens, and Quoc V Le. Randaugment: Practical automated data augmentation with a reduced search space. In *Proceedings of the IEEE/CVF conference on computer vision and pattern recognition workshops*, pages 702–703, 2020. 3
- [8] Chao Dong, Chen Change Loy, Kaiming He, and Xiaoou Tang. Image super-resolution using deep convolutional networks. *IEEE transactions on pattern analysis and machine intelligence*, 38(2):295–307, 2015. 3
- [9] Bi’an Du, Xiang Gao, Wei Hu, and Xin Li. Self-contrastive learning with hard negative sampling for self-supervised point cloud learning. In *Proceedings of the 29th ACM International Conference on Multimedia*, pages 3133–3142, 2021. 5
- [10] Michael J. Evans and Jeffrey S. Rosenthal. *Probability and statistics: Theory and applications*. 2009. 4
- [11] Haoqiang Fan, Hao Su, and Leonidas J Guibas. A point set generation network for 3d object reconstruction from a single image. In *Proceedings of the IEEE conference on computer vision and pattern recognition*, pages 605–613, 2017. 3
- [12] Gene H Golub and Christian Reinsch. Singular value decomposition and least squares solutions. In *Linear algebra*, pages 134–151. Springer, 1971. 7
- [13] Kaiming He, Xinlei Chen, Saining Xie, Yanghao Li, Piotr Dollár, and Ross Girshick. Masked autoencoders are scalable vision learners. *arXiv preprint arXiv:2111.06377*, 2021. 1
- [14] Kaiming He, Haoqi Fan, Yuxin Wu, Saining Xie, and Ross Girshick. Momentum contrast for unsupervised visual representation learning. In *Proceedings of the IEEE/CVF conference on computer vision and pattern recognition*, pages 9729–9738, 2020. 1, 2
- [15] Dan Hendrycks and Thomas Dietterich. Benchmarking neural network robustness to common corruptions and perturbations. *arXiv preprint arXiv:1903.12261*, 2019. 3
- [16] Dan Hendrycks, Norman Mu, Ekin D Cubuk, Barret Zoph, Justin Gilmer, and Balaji Lakshminarayanan. Augmix: A simple data processing method to improve robustness and uncertainty. *arXiv preprint arXiv:1912.02781*, 2019. 3
- [17] Siyuan Huang, Yichen Xie, Song-Chun Zhu, and Yixin Zhu. Spatio-temporal self-supervised representation learning for 3d point clouds. In *Proceedings of the IEEE/CVF International Conference on Computer Vision*, pages 6535–6545, 2021. 5
- [18] Feiran Li, Kent Fujiwara, Fumio Okura, and Yasuyuki Matsushita. A closer look at rotation-invariant deep point cloud analysis. In *Proceedings of the IEEE/CVF International Conference on Computer Vision*, pages 16218–16227, 2021. 7
- [19] Haotian Liu, Mu Cai, and Yong Jae Lee. Masked discrimination for self-supervised learning on point clouds. *arXiv preprint arXiv:2203.11183*, 2022. 1, 8
- [20] Ilya Loshchilov and Frank Hutter. Sgdr: Stochastic gradient descent with warm restarts. *arXiv preprint arXiv:1608.03983*, 2016. 4
- [21] Ilya Loshchilov and Frank Hutter. Decoupled weight decay regularization. *arXiv preprint arXiv:1711.05101*, 2017. 4
- [22] Mehdi Noroozi and Paolo Favaro. Unsupervised learning of visual representations by solving jigsaw puzzles. In *European conference on computer vision*, pages 69–84. Springer, 2016. 1
- [23] Yatian Pang, Wenxiao Wang, Francis EH Tay, Wei Liu, Yonghong Tian, and Li Yuan. Masked autoencoders for point cloud self-supervised learning. *ECCV*, 2022. 1, 2, 4, 8
- [24] Omid Poursaeed, Tianxing Jiang, Han Qiao, Nayun Xu, and Vladimir G Kim. Self-supervised learning of point clouds via orientation estimation. In *2020 International Conference on 3D Vision (3DV)*, pages 1018–1028. IEEE, 2020. 2, 5
- [25] Charles R Qi, Hao Su, Kaichun Mo, and Leonidas J Guibas. Pointnet: Deep learning on point sets for 3d classification and segmentation. In *Proceedings of the IEEE conference on computer vision and pattern recognition*, pages 652–660, 2017. 3, 4, 6
- [26] Charles Ruizhongtai Qi, Li Yi, Hao Su, and Leonidas J Guibas. Pointnet++: Deep hierarchical feature learning on point sets in a metric space. *Advances in neural information processing systems*, 30, 2017. 3, 4
- [27] Yongming Rao, Jiwen Lu, and Jie Zhou. Global-local bidirectional reasoning for unsupervised representation learning of 3d point clouds. In *Proceedings of the IEEE/CVF Conference on Computer Vision and Pattern Recognition*, pages 5376–5385, 2020. 2, 8
- [28] Jiawei Ren, Liang Pan, and Ziwei Liu. Benchmarking and analyzing point cloud classification under corruptions. *International Conference on Machine Learning (ICML)*, 2022. 3

- [29] Aditya Sanghi. Info3d: Representation learning on 3d objects using mutual information maximization and contrastive learning. In *European Conference on Computer Vision*, pages 626–642. Springer, 2020. 1, 2, 8
- [30] Jonathan Sauder and Bjarne Sievers. Self-supervised deep learning on point clouds by reconstructing space. *Advances in Neural Information Processing Systems*, 32, 2019. 1, 2, 5, 6
- [31] Charu Sharma and Manohar Kaul. Self-supervised few-shot learning on point clouds. *Advances in Neural Information Processing Systems*, 33:7212–7221, 2020. 6
- [32] Kihyuk Sohn, David Berthelot, Nicholas Carlini, Zizhao Zhang, Han Zhang, Colin A Raffel, Ekin Dogus Cubuk, Alexey Kurakin, and Chun-Liang Li. Fixmatch: Simplifying semi-supervised learning with consistency and confidence. *Advances in neural information processing systems*, 33:596–608, 2020. 3
- [33] Jiachen Sun, Qingzhao Zhang, Bhavya Kailkhura, Zhiding Yu, Chaowei Xiao, and Z Morley Mao. Benchmarking robustness of 3d point cloud recognition against common corruptions. *arXiv preprint arXiv:2201.12296*, 2022. 3
- [34] Yunjie Tian, Lingxi Xie, Jiemin Fang, Mengnan Shi, Junran Peng, Xiaopeng Zhang, Jianbin Jiao, Qi Tian, and Qixiang Ye. Beyond masking: Demystifying token-based pre-training for vision transformers. *arXiv preprint arXiv:2203.14313*, 2022. 2
- [35] Zhan Tong, Yibing Song, Jue Wang, and Limin Wang. Videomae: Masked autoencoders are data-efficient learners for self-supervised video pre-training. *arXiv preprint arXiv:2203.12602*, 2022. 1
- [36] Mikaela Angelina Uy, Quang-Hieu Pham, Binh-Son Hua, Thanh Nguyen, and Sai-Kit Yeung. Revisiting point cloud classification: A new benchmark dataset and classification model on real-world data. In *Proceedings of the IEEE/CVF international conference on computer vision*, pages 1588–1597, 2019. 5
- [37] Pascal Vincent, Hugo Larochelle, Yoshua Bengio, and Pierre-Antoine Manzagol. Extracting and composing robust features with denoising autoencoders. In *Proceedings of the 25th international conference on Machine learning*, pages 1096–1103, 2008. 1, 2
- [38] Hanchen Wang, Qi Liu, Xiangyu Yue, Joan Lasenby, and Matt J Kusner. Unsupervised point cloud pre-training via occlusion completion. In *Proceedings of the IEEE/CVF International Conference on Computer Vision*, pages 9782–9792, 2021. 1, 2, 4, 5, 6
- [39] Yue Wang, Yongbin Sun, Ziwei Liu, Sanjay E Sarma, Michael M Bronstein, and Justin M Solomon. Dynamic graph cnn for learning on point clouds. *Acm Transactions On Graphics (tog)*, 38(5):1–12, 2019. 3, 4, 6
- [40] Zhirong Wu, Shuran Song, Aditya Khosla, Fisher Yu, Linguang Zhang, Xiaoou Tang, and Jianxiong Xiao. 3d shapenets: A deep representation for volumetric shapes. In *Proceedings of the IEEE conference on computer vision and pattern recognition*, pages 1912–1920, 2015. 2, 5, 7
- [41] Saining Xie, Jiatao Gu, Demi Guo, Charles R Qi, Leonidas Guibas, and Or Litany. Pointcontrast: Unsupervised pre-training for 3d point cloud understanding. In *European conference on computer vision*, pages 574–591. Springer, 2020. 6
- [42] Mingye Xu, Zhipeng Zhou, Hongbin Xu, Yali Wang, and Yu Qiao. Cp-net: Contour-perturbed reconstruction network for self-supervised point cloud learning. *arXiv preprint arXiv:2201.08215*, 2022. 2
- [43] Yaoqing Yang, Chen Feng, Yiru Shen, and Dong Tian. Foldingnet: Point cloud auto-encoder via deep grid deformation. In *Proceedings of the IEEE conference on computer vision and pattern recognition*, pages 206–215, 2018. 2, 3, 4
- [44] Li Yi, Vladimir G Kim, Duygu Ceylan, I-Chao Shen, Mengyan Yan, Hao Su, Cewu Lu, Qixing Huang, Alla Sheffer, and Leonidas Guibas. A scalable active framework for region annotation in 3d shape collections. *ACM Transactions on Graphics (ToG)*, 35(6):1–12, 2016. 6
- [45] Lequan Yu, Xianzhi Li, Chi-Wing Fu, Daniel Cohen-Or, and Pheng-Ann Heng. Pu-net: Point cloud upsampling network. In *Proceedings of the IEEE conference on computer vision and pattern recognition*, pages 2790–2799, 2018. 3
- [46] Xumin Yu, Lulu Tang, Yongming Rao, Tiejun Huang, Jie Zhou, and Jiwen Lu. Point-bert: Pre-training 3d point cloud transformers with masked point modeling. *arXiv preprint arXiv:2111.14819*, 2021. 1, 2, 4, 8
- [47] Amir R Zamir, Alexander Sax, William Shen, Leonidas J Guibas, Jitendra Malik, and Silvio Savarese. Taskonomy: Disentangling task transfer learning. In *Proceedings of the IEEE conference on computer vision and pattern recognition*, pages 3712–3722, 2018. 1, 3, 4
- [48] Cheng Zhang, Jian Shi, Xuan Deng, and Zizhao Wu. Upsampling autoencoder for self-supervised point cloud learning. *arXiv preprint arXiv:2203.10768*, 2022. 2
- [49] Renrui Zhang, Ziyu Guo, Peng Gao, Rongyao Fang, Bin Zhao, Dong Wang, Yu Qiao, and Hongsheng Li. Pointm2ae: Multi-scale masked autoencoders for hierarchical point cloud pre-training. *arXiv preprint arXiv:2205.14401*, 2022. 1
- [50] Yabin Zhang, Jiehong Lin, Chenhong He, Yongwei Chen, Kui Jia, and Lei Zhang. Masked surfel prediction for self-supervised point cloud learning. *arXiv preprint arXiv:2207.03111*, 2022. 1
- [51] Yu Zhang and Qiang Yang. A survey on multi-task learning. *IEEE Transactions on Knowledge and Data Engineering*, 2021. 3
- [52] Chen Zhao, Jiaqi Yang, Xin Xiong, Angfan Zhu, Zhiguo Cao, and Xin Li. Rotation invariant point cloud analysis: Where local geometry meets global topology. *Pattern Recognition*, 127:108626, 2022. 2, 7